Crystal orientation effects on the piezoelectric field of strained zinc-blende quantum-well structures

Lars Duggen,* Morten Willatzen, and Benny Lassen
Mads Clausen Institute, University of Southern Denmark, Alsion 2, DK-6400 Sønderborg, Denmark
(Received 11 September 2008; revised manuscript received 24 October 2008; published 21 November 2008)

A three-layered zinc-blende quantum-well structure is analyzed subject to both static and dynamic conditions for different crystal growth directions taking into account piezoelectric effects and lattice mismatch. It is found that the strain component S_{zz} in the quantum-well region strongly depends on the crystal growth direction and that a piezoelectric strain contribution exists in zinc blende as in wurtzite, albeit smaller. It is also found in the absence of loss effects that resonance frequencies, giving large strains in the structure, depend strongly on the crystal growth direction. Due to the higher symmetry of the zinc-blende structure, we find in a one-dimensional model that piezoelectric effects do not affect strain values for zinc-blende structures grown along the [001] direction in contrast to the corresponding wurtzite result. However, zinc-blende structures grown along a general crystal direction show important changes in strain and the electric distribution due to piezoelectric effects. The findings indicate the quantitative importance of a fully coupled model even for zinc blende, in particular when discussing electronic band structure and optoelectronic properties.

DOI: 10.1103/PhysRevB.78.205323 PACS number(s): 77.65.Ly, 77.65.Fs

I. INTRODUCTION

Nitride based quantum-confined material combinations such as quantum-well (QW) or quantum-dot structures are promising candidates for electronic and optoelectronic applications. Hence it is important to understand the basic properties of these materials and the implications of electromechanical coupling on conduction and valence-band properties.[1] Materials such as GaN and AlN exist in both wurtzite and zinc-blende crystal classes.[2] Most work for GaN and AlN structures so far has been carried out for wurtzite crystal structures.[3–9] Jogai, Albrecht and Pan studied the effect of strain, piezoelectric effect, spontaneous polarization and surface charge on the electronic structure of quantum wells and quantum dots.[5–7] They investigated in particular the influence of solving the electromechanical problem either semicoupled, where the strain is coupled to the electric field but the electric field is not coupled to the strain, or fully coupled, where the electric field and the strain is coupled both ways. They showed that without surface charges to screen the electric field, including the full coupling gave important contributions, however, if surface charges were included the electric field strength was reduced and as a result the semicoupled model was sufficient. Park and Chuang[4] investigated the dependence of orientation on electrical and optical properties. They showed that orientation has a strong impact on among other things the piezoelectric polarization.

Zinc-blende crystal structures have received much less attention, however, it is known that zinc-blende crystal structures grown along different crystal orientations show different optoelectronic properties.[10,11] The determination of these properties is done by self-consistently solving the Schrödinger equation, Navier's equations, and Poisson's equation accounting for the stress and electric displacement constitutive relations for the system in consideration.

In this work, we address both the semicoupled and the fully coupled problem using a one-dimensional model approximation for both static and dynamic operation of zinc-blende quantum-well structures grown along arbitrary crystal orientations taking into account lattice mismatch between the quantum-well layer and the substrate.[9] The purpose of the present work is to examine whether electromechanical coupling effects (in particular influence of piezoelectric effects on strain) are also important in zinc-blende structures grown along an arbitrary crystal direction.

We also perform a frequency-dependent analysis of electromechanical couplings since zinc-blende quantum-well structures find applications in, e.g., semiconductor lasers, amplifiers, and LED's subject to dynamic operation. Special attention is given to the determination of resonance frequencies at which electromechanical effects are known to play a major role for device characteristics.

II. THEORY

The fully coupled constitutive relations for the piezoelectric effect read

$$\mathbf{T} = -\mathbf{e}^T \cdot \mathbf{E} + \mathbf{c}^{\mathbf{E}} \cdot \mathbf{S}, \tag{1}$$

$$\mathbf{D} = \boldsymbol{\epsilon}^S \cdot \mathbf{E} + \mathbf{e} \cdot \mathbf{S}, \tag{2}$$

where $\mathbf{T}$, $\mathbf{E}$, $\mathbf{S}$, and $\mathbf{D}$ are the stress tensor, electric field, strain tensor, and electric displacement, respectively. The coefficients $\mathbf{e}$, $\mathbf{c}^{\mathbf{E}}$, and $\boldsymbol{\epsilon}^S$ are the piezoelectric $\mathbf{e}$ tensor, stiffness tensor, and permittivity constant, respectively (Table I), while the superscript T denotes the matrix transpose. For the semicoupled model, $-\mathbf{e}^T$ in Eq. (1) is set to zero.

The governing equations are Navier's and Poisson's laws,

$$\nabla \cdot \mathbf{T} = \rho_m \frac{\partial^2 \mathbf{u}}{\partial t^2}, \tag{3}$$

$$\nabla \cdot \mathbf{D} = \rho_e, \tag{4}$$

where $\mathbf{u}$ is the particle displacement and the material parameters ρ_m and ρ_e denote the mass density and the free electric

 ©2008 The American Physical Society

TABLE I. Material parameters (in SI units). Parameters from Ref. 2 if not stated otherwise.

Material	e_{x4}	$c_{11}^E/10^{10}$	$c_{12}^E/10^{10}$	$c_{44}^E/10^{10}$	ϵ^S/ϵ_0	$a/10^{-10}$	ρ_m
$In_{0.1}Ga_{0.9}As$	0.149[a]	11.82	5.55	5.79	13.13[a]	5.6935	5635[b]
GaAs	0.16[a]	12.21	5.66	6.00	12.91[a]	5.6536	5307[b]
GaN	0.50[c]	29.3	15.9	15.5	9.7[c]	4.50	6150[d]
AlN	0.59[c]	30.4	16.0	19.3	9.7[c]	4.38	3245[d]
$In_{0.3}Ga_{0.7}N$	0.635[e]	26.12	14.88	13.43	11.25[e]	4.64	6348[f]
InN	0.95[e]	18.7	12.5	8.6	14.86[e]	4.98	6810[f]

[a]Reference 11.
[b]Reference 12.
[c]Reference 13.
[d]Average from References 9 and 14.
[e]Reference 15.
[f]Reference 14.

charge density, respectively. The latter is, however, assumed zero throughout this work. The strain in abbreviated subscripts[12] including the lattice mismatch reads[9]

$$\mathbf{S} = \begin{bmatrix} \frac{\partial u_x}{\partial x} - a_{\text{mis}} \\ \frac{\partial u_y}{\partial y} - a_{\text{mis}} \\ \frac{\partial u_z}{\partial z} - a_{\text{mis}} \\ \frac{\partial u_y}{\partial z} + \frac{\partial u_z}{\partial y} \\ \frac{\partial u_x}{\partial z} + \frac{\partial u_z}{\partial x} \\ \frac{\partial u_x}{\partial y} + \frac{\partial u_y}{\partial x} \end{bmatrix}, \tag{5}$$

where a_{mis} is zero in the substrate material layers, and $(a^{(2)} - a^{(1)})/a^{(1)}$ in the quantum-well layer, (2) denoting the quantum-well material and (1) the substrate material.

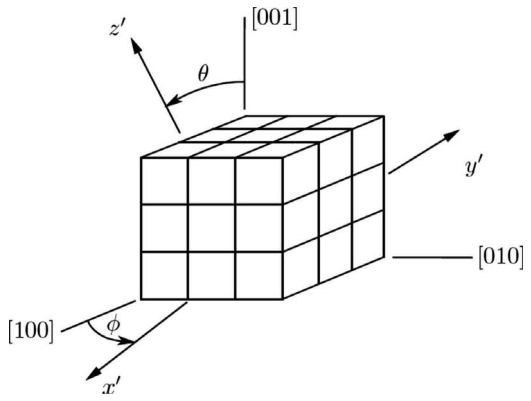

FIG. 1. Subsequent coordinate system rotations ϕ around [001] followed by θ around x'. The cubes indicate the cubic crystal structure.

The different growth directions are modeled by rotating the coordinate system such that $x \to x'$, $y \to y'$, and $z \to z'$ where the primes indicate rotated coordinates and x, y, z coincide with the crystal axis [001], [010], [100] (Fig. 1). The system boundaries then correspond to a specific z' value as seen in Fig. 2. The transformed quantities can be calculated by[12]

$$\mathbf{r}' = \mathbf{a} \cdot \mathbf{r}, \tag{6}$$

$$\mathbf{T}' = \mathbf{M} \cdot \mathbf{T}, \tag{7}$$

$$\mathbf{S}' = \mathbf{N} \cdot \mathbf{S}, \tag{8}$$

$$\mathbf{E}' = \mathbf{a} \cdot \mathbf{E}, \tag{9}$$

$$\mathbf{D}' = \mathbf{a} \cdot \mathbf{D}, \tag{10}$$

$$\boldsymbol{\epsilon}' = \mathbf{a} \cdot \boldsymbol{\epsilon} \cdot \mathbf{a}^T, \tag{11}$$

$$\mathbf{e}' = \mathbf{a} \cdot \mathbf{e} \cdot \mathbf{M}^T, \tag{12}$$

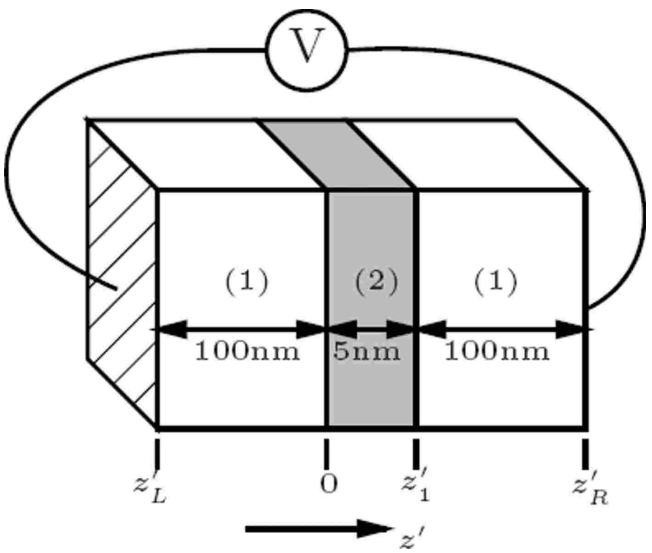

FIG. 2. Sketch of the analyzed structure.

$$\mathbf{c}^{\mathbf{E}'} = \mathbf{M} \cdot \mathbf{c}^{\mathbf{E}} \cdot \mathbf{M}^T, \tag{13}$$

where $\mathbf{r}$ denotes the position vector and the transformation matrix $\mathbf{a}$ reads[16]

$$\mathbf{a} = \begin{bmatrix} \cos(\phi) & \sin(\phi) & 0 \\ -\cos(\theta)\sin(\phi) & \cos(\theta)\cos(\phi) & \sin(\theta) \\ \sin(\theta)\sin(\phi) & -\sin(\theta)\cos(\phi) & \cos(\theta) \end{bmatrix}, \tag{14}$$

with θ, ϕ as the Eulerian angles, and the Bond stress and strain transformation matrices $\mathbf{M}$ and $\mathbf{N}$ are constructed by elements of $\mathbf{a}$ as given in Ref. 12 (p. 74). It should be noted that $\mathbf{N}^{-1}=\mathbf{M}^T$ and $\mathbf{a}^{-1}=\mathbf{a}^T$. For simplicity, it is now assumed that all fields are functions of z' only. As mentioned above, the free charge carrier density ρ_e is assumed to be zero; i.e., we neglect charge screening at material interfaces. Finally it is assumed that the embedding material is vacuum, such that the stresses at all surfaces are zero.

A. Static case

In the static case, Navier's law applied in each separate layer becomes

$$\frac{\partial T_5'}{\partial z'} = \frac{\partial T_4'}{\partial z'} = \frac{\partial T_3'}{\partial z'} = 0. \tag{15}$$

Using Eqs. (1) and (2) along with D_z' being constant in space and the definition of strain yields

$$\frac{\partial^2 u_x'}{\partial z'^2} = \frac{\partial^2 u_y'}{\partial z'^2} = \frac{\partial^2 u_z'}{\partial z'^2} = 0. \tag{16}$$

Since, in the electrostatic case, $\nabla \times \mathbf{E}=0$, we can introduce the electric potential Φ such that $-\nabla\Phi=\mathbf{E}$. Using Eq. (2) with D_z' and $\mathbf{S}'$ being constant in space [as follows from Eq. (16)], we have

$$\frac{\partial^2 \Phi}{\partial z'^2} = 0. \tag{17}$$

Hence, the solutions for the particle displacements u_x', u_y', and u_z' and the electric potential Φ read

$$\begin{cases} \mathcal{A}_i^{(1)} z' + \mathcal{B}_i^{(1)}, & z_L' \le z' \le 0 \\ \mathcal{A}_i^{(2)} z' + \mathcal{B}_i^{(2)}, & 0 \le z' \le z_1' \\ \mathcal{A}_i^{(3)} z' + \mathcal{B}_i^{(3)}, & z_1' \le z' \le z_R', \end{cases} \tag{18}$$

with $i=x,y,z$, and Φ for the different solutions, respectively. The coefficients $\mathcal{A}$ and $\mathcal{B}$ are found by applying continuity of

$$T_3', T_4', T_5', u_x', u_y', u_z', D_z', \text{ and } \Phi \tag{19}$$

everywhere (in particular at the material interfaces), and at the outer boundaries ($z'=z_L', z_R'$):

$$T_5' = T_4' = T_3' = 0, \quad D_z' = D, \tag{20}$$

where D is an externally applied electric displacement. Finally the reference values for Φ and $\mathbf{u}'$ are free of choice. For convenience, we choose

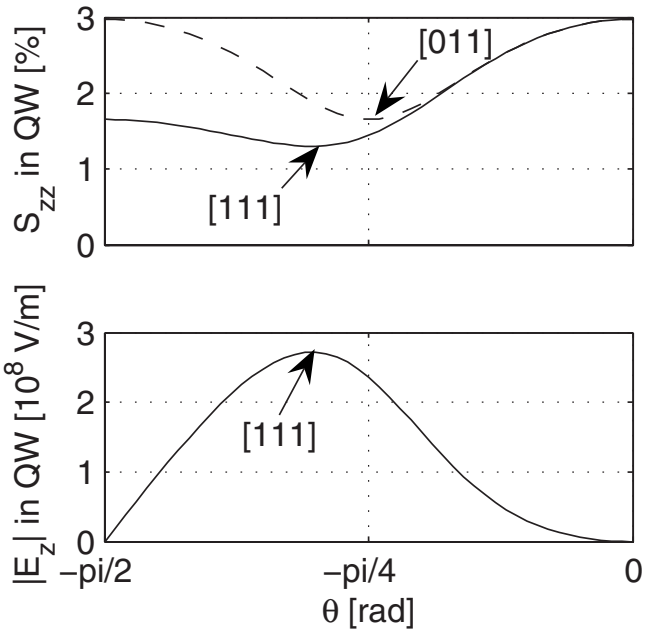

FIG. 3. Strain and electric field in the quantum well vs crystal rotation for $D_z'=0$ corresponding to open-circuit conditions in AlN/GaN. Dashed and solid lines indicate $\phi=0$ and $\phi=-\pi/4$, respectively.

$$\mathbf{u}|_{z'=0} = 0, \quad \Phi|_{z'=z_R'} = 0.$$

The strain component S_{zz}' as well as the electric field in the quantum-well vs crystal growth direction for $D=0$ can be seen in Fig. 3.

As seen in Fig. 3, the strain component S_{zz}' depends strongly on the crystal growth direction with $S_{zz}'([111])$ being 45% of $S_{zz}'([001])$. On the other hand, a large electric field is induced in the [111] growth direction. Analog calculations have been carried out using the semicoupled model for which $\mathbf{e}^T=0$ in Eq. (1).

In order to compare the fully and semicoupled models, the strain is split up into two parts:

$$\mathbf{S}_{\text{fully coupled}} = \mathbf{S}_{\text{semicoupled}} + \mathbf{S}_{\text{coupling}}. \tag{21}$$

The relative deviation is expressed as $\mathbf{S}_{\text{coupling}}/\mathbf{S}_{\text{fully coupled}}$. It is found that the relative deviation is largest along the [111] growth direction. We find the fully coupled compressional strain for [111]-grown structures,

$$S_{zz}' = \frac{2\sqrt{3}\frac{e_{x4}^{(2)}}{\epsilon^{(2)}} D + 3(c_{11}^{(2)} + 2c_{12}^{(2)}) a_{\text{mis}}}{4\frac{e_{x4}^{(2)^2}}{\epsilon^{(2)}} + c_{11}^{(2)} + 2c_{12}^{(2)} + 4c_{44}^{(2)}} - a_{\text{mis}}. \tag{22}$$

Results for different material compositions are given in Table II where we also compare the found electric field with experimental values.[11,17] It should be noted that the experiments carried out by Ref. 17 are misoriented by 1° from [111] toward [211] while the theoretical results are for the

TABLE II. Contributions to S'_{zz} in the [111]-grown QW layer for different material compositions with $D=0$, corresponding to open-circuit conditions. For GaAs/$In_xGa_{1-x}As$ both $E_{z,t}$ and $E_{z,e}$, being the theoretical and the experimental electric field in the QW layer, respectively, are listed for comparison.

Substrate/QW	S_{semi}	S_{coupling}	Deviation	$E'_{z,t}$ $(V/\mu\text{m})$	$E'_{z,e}$ $(V/\mu\text{m})$
GaAs/$In_{0.1}Ga_{0.9}As$	0.34%	−0.002%	0.5%	15.56	17 ± 1 [a]
GaAs/$In_{0.2}Ga_{0.8}As$	0.710%	−0.003%	0.4%	28.63	25[b]
AlN/GaN	1.34%	−0.04%	3.1%	271.6	
GaN/$In_{0.3}Ga_{0.7}N$	1.69%	−0.07%	4.4%	355.0	
GaN/InN	7.24%	−0.61%	−9.1%	1441.5	
GaN/AlN	−0.91%	0.04%	−4.7%	−280.3	

[a]Reference 11.
[b]Reference 17.

ideal [111]-growth direction. Thus the difference between the theoretical and experimental result is slightly less than given in Table II.

As seen, the quality of the semicoupled model depends on the specific material composition and is generally better than for wurtzite-based QW structures.[9] More specifically it depends on the ratio between e_{x4}^2/ϵ and the stiffness parameters as well as a_{mis}. For InN the stiffness parameters are comparably small while e_{x4} is comparably large and the mismatch with GaN is comparably large. Thus, the deviation in zinc-blende GaN/AlN is 4.7% while the corresponding deviation for wurtzite is much larger (the pure piezoelectric contribution to strain along the [001] growth direction is approximately 18% for wurtzite GaN/AlN). Although when GaN/InN is considered, the deviation becomes significantly larger and it is expected that this will lead to notable deviations in the electronic structure affecting optoelectronic properties.[4,18] However a classical mechanical description is somewhat dubious for smaller GaN/InN QW structures accommodating large mismatch strain effects.

B. Dynamic case

Next, the dynamic case is considered. Differentiating the definition of strain with respect to time and combining this with Navier's law yields

$$\frac{\partial^2 T'_5}{\partial z'^2} = \rho_m \frac{\partial^2 S'_5}{\partial t^2}, \tag{23}$$

$$\frac{\partial^2 T'_4}{\partial z'^2} = \rho_m \frac{\partial^2 S'_4}{\partial t^2}, \tag{24}$$

$$\frac{\partial^2 T'_3}{\partial z'^2} = \rho_m \frac{\partial^2 S'_3}{\partial t^2}. \tag{25}$$

Rewriting Eq. (2) and inserting into Eq. (1) gives

$$\mathbf{T}' = -\mathbf{e}'^T\left(\frac{\mathbf{D}' - \mathbf{e}'\mathbf{S}'}{\epsilon^S}\right) + \mathbf{c}^{\mathbf{E}'}\mathbf{S}'. \tag{26}$$

Employing the frequently used electrostatic approximation[12] leads to $E'_x=E'_y=0$, and Eq. (2) gives $D'_x=(\mathbf{e}'\mathbf{S}')_1$ and $D'_y=(\mathbf{e}'\mathbf{S}')_2$. Then, we can express $\mathbf{T}'$ component-wise as

$$T'_i = -e'^T_{i3}\left(\frac{D'_z - (\mathbf{e}'\mathbf{S}')_3}{\epsilon^S}\right) + (\mathbf{c}^{\mathbf{E}'}\mathbf{S})_i, \tag{27}$$

which is the same as Eq. (26) when modifying $\mathbf{e}'^T$ by setting the first two columns to zero. Inserting in Eqs. (23)–(25) yields three coupled wave equations for stress:

$$\frac{\gamma_{33}}{\rho_m}\frac{\partial^2 T'_3}{\partial z'^2} + \frac{\gamma_{34}}{\rho_m}\frac{\partial^2 T'_4}{\partial z'^2} + \frac{\gamma_{35}}{\rho_m}\frac{\partial^2 T'_5}{\partial z'^2} - \frac{\partial T'_3}{\partial t^2} = \frac{e'^T_{3z}}{\epsilon^S}\frac{\partial^2 D'_z}{\partial t^2}, \tag{28}$$

$$\gamma_{43}\frac{\partial^2 T'_3}{\partial z'^2} + \gamma_{44}\frac{\partial^2 T'_4}{\partial z'^2} + \gamma_{45}\frac{\partial^2 T'_5}{\partial z'^2} - \rho_m\frac{\partial T'_5}{\partial t^2} = \rho_m\frac{e'^T_{4z}}{\epsilon^S}\frac{\partial^2 D'_z}{\partial t^2}, \tag{29}$$

$$\gamma_{53}\frac{\partial^2 T'_3}{\partial z'^2} + \gamma_{54}\frac{\partial^2 T'_4}{\partial z'^2} + \gamma_{55}\frac{\partial^2 T'_5}{\partial z'^2} - \rho_m\frac{\partial T'_5}{\partial t^2} = \rho_m\frac{e'^T_{5z}}{\epsilon^S}\frac{\partial^2 D'_z}{\partial t^2}, \tag{30}$$

where γ denotes the modified effective stiffness

$$\gamma = \frac{\mathbf{e}'^T_{\mathbf{m}}\cdot\mathbf{e}'}{\epsilon^S} + \mathbf{c}^{\mathbf{E}'}, \tag{31}$$

and $\mathbf{e}'^T_{\mathbf{m}}$ being $\mathbf{e}'^T$ with the first two columns set to zero [refer to discussion following Eq. (27)]. It has been checked that γ indeed is symmetric.

1. Monofrequency case

In the monofrequency case, an external voltage $\propto\exp(i\omega t)$ is applied and the dispersion curves are obtained by assuming harmonic solutions $T\propto\exp(i(\omega t+kz'))$ and then solving the homogeneous linear equation system. Here it should be noted that acoustic vibrations depend on the piezoelectric elements e'^T_{3z}, e'^T_{4z}, e'^T_{5z}. For [001]-grown zinc-blende quantum wells they will all be zero and no resonances exists. In the case of the [011] and [111] growth directions, only the x and z' polarization will be excited, respectively.

Solutions consist of forward and backward propagating waves. The solution for the x' polarizations reads [omitting the trivial factor $\exp(i\omega t)$]:

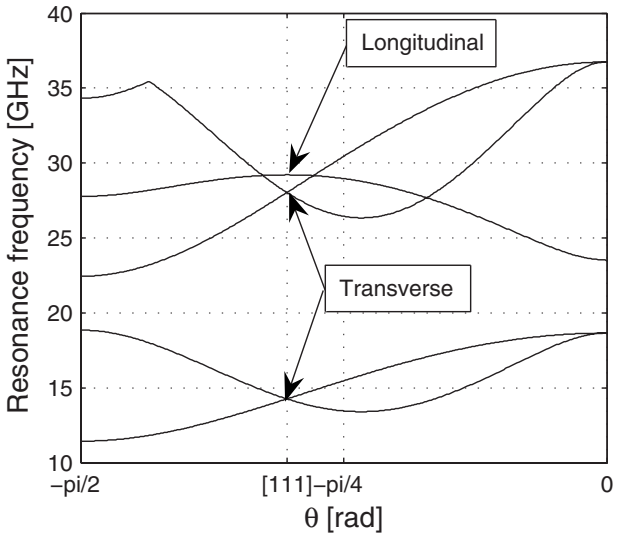

FIG. 4. The first five resonance frequencies for the AlN/GaN structure with $\phi=-\pi/4$.

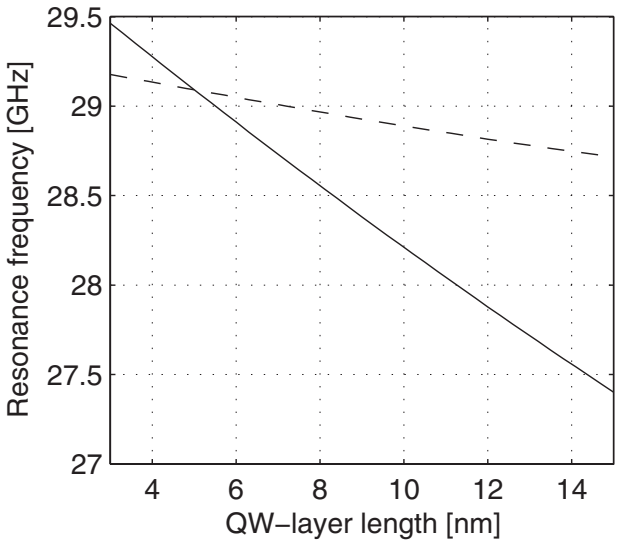

FIG. 5. Resonance frequency for the longitudinal wave as function of QW-layer length at [111]-growth direction. The solid curve describes the case where the substrate layers each remain 100 nm long, while the dashed curve describes the case where the QW-layer length is varied but the total structure is kept at a constant length of 205 nm.

$$T_5' = \mathcal{T}_{5A+}\exp(ik_1z') + \mathcal{T}_{5A-}\exp(-ik_1z') + \mathcal{T}_{5B+}\exp(ik_2z') + \mathcal{T}_{5B-}\exp(-ik_2z') + \mathcal{T}_{5C+}\exp(ik_3z') + \mathcal{T}_{5C-}\exp(-ik_3z') - \frac{e_{5z}'^{T}}{\epsilon^{S}}D_z'. \quad (32)$$

The other two polarizations are found by solving the dispersion relation for $T_3'/T_5'(k)$ and $T_4'/T_5'(k)$. With these amplitude relations, all stress amplitudes are given by the six T_5' amplitudes.

The boundary conditions for the monofrequency analysis are the same as in the static case since continuity of particle displacement automatically implies continuity of particle velocity. The particle velocity can be expressed by $\mathbf{T}$ as

$$\mathbf{v}' = \frac{\pm k}{\omega\rho_m}\mathbf{T}', \quad (33)$$

where the sign depends on the propagation direction.

In the general case, application of boundary conditions results in an 18×18 linear equation system with $\exp(\pm ikz_L')$, $\exp(\pm ikz_R')$, $\exp(\pm ikz_1')$ terms as coefficients and $\mathcal{T}_{5A,B,C\pm}$ as unknowns—see also Ref. 9 for a simple example on wurtzite structures. Resonance frequencies are found by setting the determinant of the coefficient matrix to zero.

Indicated in Fig. 4 is the crystal growth direction [111] where the transverse wave polarizations are decoupled from the longitudinal ones. For the [111] growth direction, only longitudinal waves are generated due to electric excitation [as follows from Eqs. (28)–(30), where the corresponding γ coefficients become zero]. On the other hand, for all crystal growth directions near [111] all polarization directions are excited and coupled.

Thus, depending on the energy dissipation in the structure (considered to be zero here), one has to be cautious when calculating resonance frequencies using an ideal model for the [111]-growth direction not taking into account transverse wave polarizations, since defects in the lattice might perturb this direction and cause resonance at significantly lower frequencies than predicted.

Finally, the impact of size effects is shown in Fig. 5. The latter figure indicates, as expected, that a change in total structure length has a much larger influence on the resonance frequencies than the actual length of the QW layer if the total structure is kept at a constant length. We also see, as expected, that the resonance frequencies decrease with increasing length.

III. CONCLUSIONS

A one-dimensional model describing electromechanical fields due to piezoelectricity and lattice mismatch in zinc-blende quantum-well structures has been derived and solved for several material compositions and different crystal growth directions. It is shown that, in the static case, the strain as well as the piezoelectric component depends strongly on the crystal growth direction. As opposed to wurtzite AlN/GaN QW structures, the piezoelectric component in AlN/GaN remains comparably small, although it is still much larger than for zinc-blende InGaAs/GaAs. As opposed to wurtzite AlN/GaN, the contribution from piezoelectric effects to strain in zinc-blende AlN/GaN is small, yet it is larger than for zinc-blende InGaAs/GaAs quantum-well structures.

It is also shown that the resonance frequencies depend strongly on the crystal growth direction. The [111] growth direction is a special situation where only the longitudinal wave polarization is excited. Other wave polarizations have significantly lower resonance frequencies that might need to be taken into account when considering practical situations where defects in the crystal structure may be present.

*duggen@mci.sdu.dk

[1] J. Singh, *Electronic and Optoelectronic Properties of Semiconductor Structures*, 1st ed. (Cambridge University Press, Cambridge, 2003).
[2] I. Vurgaftman, J. R. Meyer, and L. R. Ram-Mohan, J. Appl. Phys. **89**, 5815 (2001).
[3] J. Wang, J. B. Jeon, Yu. M. Sirenko, and K. W. Kim, IEEE Photonics Technol. Lett. **9**, 728 (1997).
[4] S. H. Park and S. L. Chuang, Phys. Rev. B **59**, 4725 (1999).
[5] E. Pan, J. Appl. Phys. **91**, 3785 (2002).
[6] B. Jogai, J. Appl. Phys. **91**, 3721 (2002).
[7] B. Jogai, J. D. Albrecht, and E. Pan, J. Appl. Phys. **94**, 3984 (2003).
[8] U. M. E. Christmas, A. D. Andreev, and D. A. Faux, J. Appl. Phys. **98**, 073522 (2005).
[9] M. Willatzen, B. Lassen, L. C. L. Y. Voon, and R. V. N. Melnik, J. Appl. Phys. **100**, 024302 (2006).
[10] T. Ohtoshi, A. Niwa, and T. Kuroda, IEEE J. Sel. Top. Quantum Electron. **4**, 527 (1998).
[11] E. Caridi, T. Chang, K. Goossen, and L. Eastman, Appl. Phys. Lett. **56**, 659 (1990).
[12] B. Auld, *Acoustic Fields and Waves in Solids*, 2nd ed. (Krieger, Malabar, FL, 1990), Vol. 1.
[13] V. A. Fonoberov and A. A. Balandin, J. Appl. Phys. **94**, 7178 (2003).
[14] V. Chin, T. Tansley, and T. Osotchan, J. Appl. Phys. **75**, 7365 (1994).
[15] S. Y. Davydov, Semiconductors **36**, 41 (2002).
[16] H. Goldstein, *Classical Mechanics*, 2nd ed. (Addison-Wesley, Reading, MA, 1980).
[17] J. I. Izpura, J. J. Sánchez, J. L. Sánchez-Rojas, and E. Muñoz, Microelectron. J. **30**, 439 (1999).
[18] V. M. Fomin, V. N. Gladilin, S. N. Klimin, J. T. Devreese, N. A. J. M. Kleemans, and P. M. Koenraad, Phys. Rev. B **76**, 235320 (2007).